ACS OMEGA

http://pubs.acs.org/journal/acsodf

Article

Laser-Assisted Surface Modification of Ni Microstructures with Au and Pt toward Cell Biocompatibility and High Enzyme-Free Glucose Sensing

Evgeniia M. Khairullina, Ilya I. Tumkin,* Daniil D. Stupin, Alexandra V. Smikhovskaia, Andrey S. Mereshchenko, Alexey I. Lihachev, Andrey V. Vasin, Mikhail N. Ryazantsev, and Maxim S. Panov

Cite This: *ACS Omega* 2021, 6, 18099−18109

Read Online

ACCESS | Metrics & More | Article Recommendations

ABSTRACT: We investigated the influence of morphology of Ni microstructures modified with Au and Pt on their cell biocompatibility and electrocatalytic activity toward non-enzymatic glucose detection. Synthesis and modification were carried out using a simple and inexpensive approach based on the method of laser-induced deposition of metal microstructures from a solution on the surface of various dielectrics. Morphological analysis of the fabricated materials demonstrated that the surface of the Ni electrode has a hierarchical structure with large-scale 10 μm pores and small-scale 10 nm irregularities. In turn, the Ni-Pt surface has large-scale cavities, small-scale pores (1−1.5 μm), and a few tens of nanometer particles opposite to Ni-Au that reveals no obvious hierarchical structure. These observations were supported by impedance spectroscopy confirming the hierarchy of the surface topography of Ni and Ni-Pt structures. We tested the biocompatibility of the fabricated Ni-based electrodes with the HeLa cells. It was shown that the Ni-Au electrode has a much better cell adhesion than Ni-Pt with a more complex morphology. On the contrary, porous Ni and Ni-Pt electrodes with a more developed surface area than that of Ni-Au have better catalytic performance toward enzymeless glucose sensing, revealing greater sensitivity, selectivity, and stability. In this regard, modification of Ni with Pt led to the most prominent results providing rather good glucose detection limits (0.14 and 0.19 μA) and linear ranges (10−300 and 300−1500 μA) as well as the highest sensitivities of 18,570 and 2929 μA mM^{-1} cm^{-2}. We also proposed some ideas to clarify the observed behavior and explain the influence of morphology of the fabricated electrodes on their electrocatalytic activity and biocompatibility.

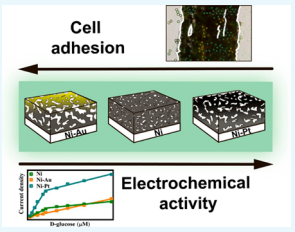

INTRODUCTION

Development and fabrication of new electrocatalytically active materials sensitive to various biologically important substances are extremely important for medicine, including the diagnosis of a large number of serious diseases.[1,2] One of such compounds is glucose; in turn, accurate and rapid determination of its concentration in the blood is extremely important for diagnosis and prevention of many diseases, including atherosclerosis, Parkinson's disease, diabetes, and others.[3,4] Most often, optical and electrochemical methods or methods representing a combination of them are used to determine the concentration of glucose in the human blood or model solutions.[5,6] Typically, the electrochemical determination of the glucose concentration, as the most frequently used method in this regard, can occur either through its enzymatic cleavage followed by the corresponding redox reactions or by its electrocatalytic oxidation directly on the electrode surface.[7] The first approach has a number of disadvantages such as the high cost of enzymes, their tendency for relatively fast decomposition, and high dependence on the environmental conditions,[8] which makes it less attractive compared to the enzyme-free approach.[9] As a rule, enzyme-free sensors are metallic or composite materials, the sensory activity of which is higher due to the presence of a greater number of active centers on their surface.[10]

There are many techniques allowing us to fabricate such materials; however, we would like to highlight only those that deal with laser-induced processes and we would also like to show their benefits in comparison with others. The main advantages of the laser-assisted methods are expressiveness, possibility to metallize different types of surfaces, opportunity to manufacture the metallic structures of different geometry, and a small number of reagents used for synthesis.[11] Such methods include direct laser writing,[12,13] selective laser sintering,[14] laser interference lithography,[15] laser pattering,[16]

Received: April 9, 2021
Accepted: June 16, 2021
Published: July 2, 2021

Table 1. Composition of Solutions Used for Laser-Assisted Fabrication of Ni-, Au-, and Pt-Based Microstructures

Electrode material	Reagent	Concentration (mM)	Solvent
Ni	nickel(II) chloride hexahydrate ($NiCl_2 \cdot 6H_2O$)	2	H_2O
	potassium sodium tartrate tetrahydrate ($KNaC_4H_4O_6 \cdot 4H_2O$)	7	
	sodium hydroxide (NaOH)	10	
Au	chloro(triphenylphosphine)gold(I) ($(Ph_3P)AuCl$)	1	*N*,*N*-dimethylformamide (DMF)
Pt	dichloro(dicyclopentadienyl)platinum(II) ($C_{10}H_{12}Cl_2Pt$)	1	*N*,*N*-dimethylformamide (DMF)

pulsed laser ablation,[17] and others. In this work, we used another technique belonging to laser technologies, which is based on a process of the laser-induced metal deposition from a solution (LCLD). In this method, laser light activates the surface of a dielectric and accelerates metal deposition within the irradiated area by increasing the temperature in the local volume at the vicinity of the focus of a laser beam.[18] The high intensity of the focused laser beam creates locally highly non-equilibrium states with high temperature and concentration gradients. As a rule, it is assumed that the mechanism of the laser-induced metal deposition reaction is similar to the autocatalytic mechanism that can proceed via either thermo- or photoinduced regimes. The main groups of factors that can affect the laser-assisted deposition of metals include physical (laser wavelength, laser power, scanning speed, and temperature), chemical (solution composition, component concentrations, pH, and chemical reactions involved in the reaction), and surface properties of the dielectric substrate (structure, the presence of activated and catalytic sites, roughness, phase composition, and the chemical properties of the dielectric components). LCLD was capable of producing quite an amount of electrode materials based on copper, nickel, cobalt, molybdenum, iridium, gold, platinum, and ruthenium; moreover, most of them have revealed rather good glucose-sensing activity.[19−25] It should be noted here that the major strength of this method is its ability to synthesize metallic and bimetallic microstructures with a highly developed surface area and, therefore, with high electrocatalytic activity. In turn, it is known that the most challenging tasks facing the scientific community are to improve the selectivity, stability, and biocompatibility of new non-enzymatic glucose sensors as well as to increase their sensing activity.[26] As an option, it can be done by increasing the surface area of the electrode material through its modification with nanosized structures. In general, this modification can be carried out, for example, by nanoparticles of precious metals, e.g., gold and platinum, chemically synthesized or obtained by photochemical reduction of their complexes.[27−29] Indeed, implementation of the unique properties of three-dimensional structures with a large surface area of such catalytically active and biologically compatible metals as gold and platinum may significantly reduce analysis time and enhance the electrocatalytic activity of an enzyme-free electrode with respect to glucose sensing.[10,30] Alternatively, a similar effect can be achieved using electrode materials based on bi- or polymetallic structures manufactured by co-deposition of two or several metals upon laser irradiation.[22,24]

As a result, in this work, we have fabricated two microcomposites using laser-induced deposition of gold and platinum on the surface of pre-synthesized nickel microstructures. It is known that many transition metals have proven to be excellent materials for enzyme-free sensors due to their good catalytic performance. Among them, nickel is of particular interest as the most intensively investigated economic catalyst for the oxidation of organic compounds, including glucose.[31] Typically, glucose oxidation by nickel and other transition metal catalysts involves redox reactions between metal hydroxides and their oxyhydroxides ($Ni(OH)_2$/NiOOH, in the case of nickel).[10,31] Briefly, the mechanism of glucose electrooxidation on the surface of a nickel electrode can be presented as follows. The catalytically active NiOOH reduces to $Ni(OH)_2$ by hydrogen abstracted from the C_1 position of glucose. Then, the generated radical species oxidizes to glucono-δ-lactone and undergoes subsequent hydrolysis, forming gluconic acid.[10] Even though nickel is arguably one of the most sensitive electrode materials for non-enzymatic sensing and nickel-based electrodes demonstrate the outstanding long-term stability, it has a number of severe disadvantages mostly related to low selectivity and limitations of their implementation in the physiological solutions (pH = 7.4). These limitations are mostly related to the fact that NiOOH catalysis strongly depends on the concentration of OH^- in the studied medium.[9] On the other hand, as it was already mentioned, the polymetallic sensor platforms, e.g., based on alloys and adatoms, opposite to monometallic sensors may drastically stimulate the process of the electrocatalytic oxidation of glucose due to the synergetic effect between metals included in their compositions.[32−34] For example, bimetallic systems containing such biologically compatible metals as gold and platinum in combination with transition metals can substantially enhance catalytic properties and provide better long-term activity of these systems.[35−37] It should also be noted here that, despite the high selectivity of pure gold and platinum electrodes used for enzyme-free glucose sensing, they have some crucial drawbacks mostly associated with their high cost and affinity to undergo poisoning (self-poisoning as well) from many oxidation products, including chlorine anions, especially in the physiological environment.[9,10] In contrast, the composites with lower amounts of precious metals could be a good choice to surpass the limitations related to usage of the electrode materials based on pure metals mentioned above and may improve the sensitivity and selectivity of the corresponding electrodes toward non-enzymatic glucose sensing. There are numerous examples of Au- and Pt-based hierarchical structures used as low-cost disposable electrodes for glucose monitoring with decent electrochemical characteristics.[38−42] Nevertheless, most of these highly promising glucose-sensing platforms suffer from insufficient efficiency and electrocatalytic activity, which give grounds for their further development primarily to improve their selectivity, stability, and biocompatibility.

MATERIALS AND METHODS

Reagents and Fabrication of Microstructures Based on Ni, Au, and Pt. All reagents used in this work were commercially available (Sigma-Aldrich, St. Louis, MO, USA) and analytical grade. The solution compositions for laser-

https://doi.org/10.1021/acsomega.1c01880
ACS Omega 2021, 6, 18099−18109

assisted fabrication of electrodes containing nickel, gold, and platinum can be found in Table 1. These electrodes were deposited on the surface of glass.

The experimental setup for the synthesis of the electrode materials using the LCLD technique is illustrated in Figure 1.

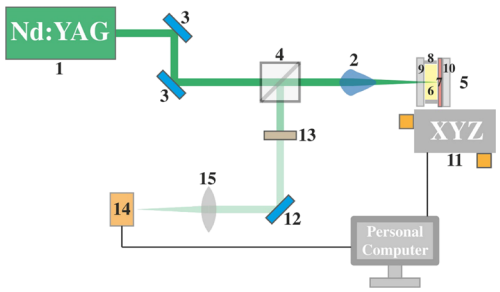

Figure 1. Basic block scheme of the experimental setup for laser-induced deposition of Ni-, Au-, and Pt-based microstructures.

Shortly, the fabrication procedure can be described as follows. The output from a diode-pumped continuous-wave solid-state Nd:YAG laser (**1**) (Changchun, China) operating at 532 nm is split in two parts. The first part of the laser output was sent to a standard microscope objective (**2**) with a focal length of 15 mm using two aluminum mirrors (**3**) and an optical separation cube (**4**). Then, it was focused on the experimental cell (**5**) within the area between a solution (**6**) and a dielectric substrate (**7**, glass). The size of the focused laser spot was about 5 μm. This cell (**5**) represents a silicone ring (**8**, 5 mm thick) with a hole on top for a solution injection sandwiched between a glass plate (**9**, in the front) and a dielectric substrate (**7**) followed by another glass plate in the back (**10**). In turn, **5** can be moved in three dimensions by a computer-controlled XYZ-motorized stage (**11**) to produce metallic microstructures of different shapes and sizes. At the same time, the second part of the laser output, which can be considered as a reflection of the first part from **5**, travels to an optical separation cube (**4**) with subsequent redirection toward the aluminum mirror (**12**). The intensity of the second portion of the 532 nm light is attenuated using a neutral density (ND, fractional transmittance 25%) filter (**13**). Further, after the mirror, the laser beam was focused on a web camera (**14**) using a short focusing lens (**15**, f = 10 cm) for monitoring and regulating the deposition process.

In the beginning, we deposited the ∼10 mm-long and ∼150 μm-wide nickel lines (or electrodes) at a laser power density of ∼2.5 mW μm^{-2} and at a scanning speed of 5 μm s^{-1}. Then, we fabricated nickel-gold and nickel-platinum electrodes by laser-induced deposition of gold and platinum on the surface of the pre-synthesized nickel lines at a laser power density of ∼2.4 mW μm^{-2} and at a scanning speed of 5 μm s^{-1}, in both cases.

Morphology Characterization/Elemental and Phase Composition Analysis. The surface morphology of the synthesized electrode materials was investigated using a scanning electron microscope JSM-7001F (JEOL, Japan). The scanning electron microscopy (SEM) images were obtained in the secondary electron mode with a beam voltage of 5 kV. The elemental composition of these electrodes was evaluated by the electron microprobe (EMP) technique also on the JSM-7001F scanning electron microscope using an energy-dispersive analyzer INCA PentaFETx (Oxford Instruments, England). Line identification was performed automatically using JOEL-7001F microscope software. The pore size distribution was estimated by manual pore counting on the SEM images.

Energy-dispersive X-ray spectroscopy (EDX) was applied to identify the atomic composition of microelectrodes using an INCA X-Act EDX analyzer (Oxford Instruments, UK) coupled with SEM.

To identify the phase composition of the fabricated electrodes, X-ray diffraction analysis (XRD) was carried out on a Bruker D2 Phaser diffractometer equipped with a LynxEye detector (Bruker-AXS, Karlsruhe, Germany) using CuKα (0.1542 nm) radiation in the 2θ angle range of 0−100°.

Impedance Spectroscopy. The impedance spectra were recorded using a homemade setup based on the high-speed and high-resolution Fourier-electrochemical impedance spectroscopy (EIS) method.[43] All measurements were performed with a 15 mV sweep-shape excitation voltage in the frequency range of 100 Hz to 40 kHz with a 2 Hz resolution. We had a two-electrode electrochemical cell with the synthesized microstructures used as the working electrode and the platinum electrode with a large area used as a reference. Both electrodes were embedded into glass containing 0.9% NaCl solution (Biolot, Saint Petersburg, Russia). The impedance spectra approximation by the complex non-linear least-squares (CNLS) method[44] was done in the NELM package for MATLAB[43] (can be obtained by request). Figure 2

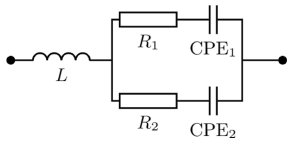

Figure 2. Equivalent scheme for evaluation of the fabricated electrodes. Here, $L \approx$ fH is the parasitic inductance caused by the finite-time response of the ammeter.

illustrates the equivalent scheme used for CNLS spectra analysis. Here, CPE is the constant phase element;[45] the impedance of which equals to

$$Z = \frac{1}{W(i\omega)^{\alpha}}$$

where α is the non-ideality parameter and W is the pseudocapacitance with dimension S s$^{\alpha}$. In general, CPE elements describe non-ideal capacitors. In particular, the $\alpha \approx$ 0.5 can be attributed to the interface between an electrolyte and an electrode with the developed (porous) surface.[46−48] For taking into account the delay between excitation voltage and current response measurements by ADC, the parameter Δt was introduced in the model as follows:

$$Y_m = Y_s \times e^{i\omega\Delta t}$$

where Y_m is the model, which was implemented for CNLS approximation, Y_s is the admittance (Figure 2), and ω is the angular frequency. For statistics reasons, the measurements were repeated 10 times.

Biocompatibility Studies. For biocompatibility studies, the HeLa cells[49] were seeded on the surface of the fabricated materials. These cells were obtained from the Bank of Cell Cultures of the Institute of Cytology of the Russian Academy of Sciences. The electrodes with cells were incubated 24 h at 37 °C and 5% CO_2 in DMEM (Dulbecco's modified Eagle's

https://doi.org/10.1021/acsomega.1c01880
ACS Omega 2021, 6, 18099−18109

medium, Biolot, Saint Petersburg, Russia) solutions with 10% fetal bovine serum (Biolot, Saint Petersburg, Russia) and 40 μg mL^{-1} gentamicin. Before microscopic investigation, the HeLa cells were treated with a dibenzoazacyclooctyne (DIBAC) fluorescent dye (membrane visualization, Thermo Fisher Scientific, USA). Then, the cell medium was replaced with phosphate saline buffer (Biolot, Saint Petersburg, Russia) with the addition of a propidium iodide dye (for dead cell nuclei visualization). The cell images were taken on a Leica DMB-4000 microscope (Leica, Germany) and presented in pseudo-color. Here, images taken in the visible range of the transmitted light were in black and white color, whereas green and red channels were attributed to DIBAC and propidium iodide fluorescence, respectively. The concentration of the propidium iodide dye was 10 μg mL^{-1}, which was enough for dyeing the dead cell monolayer.

Electrochemical Measurements. The electrochemical characteristics of the fabricated electrodes were obtained using voltammetric methods. These experiments were conducted using an Elins P30I potentiostat (Electrochemical Instruments Ltd., Chernogolovka, Russia) at an ambient temperature in a standard three-electrode cell (Figure 3), in which the platinum

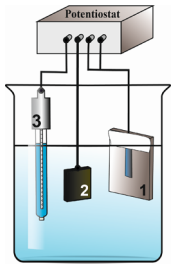

Figure 3. Three-electrode electrochemical cell used for investigation of the electrochemical properties of the fabricated Ni-based microstructures. Here, 1, working electrode (Ni, Ni-Au, or Ni-Pt); 2, counter electrode; 3, reference electrode.

wire, Ag/AgCl electrode, and the synthesized microstructures were used as counter, reference, and working electrodes, respectively. Cyclic voltammetric measurements were carried out at a scan rate of 50 mV s^{-1} between −0.9 and 0.9 V vs Ag/AgCl. Amperometric responses were recorded by the addition of D-glucose (GL) of various concentrations to the background solution (0.1 M NaOH) with simultaneous stirring. The selectivity of non-enzymatic glucose sensing of the studied electrodes was tested in the presence of ascorbic acid (AA), uric acid (UA), 4-acetamidophenol (AP), and hydrogen peroxide (H_2O_2) used as the interfering analytes.

RESULTS AND DISCUSSION

First, we optimized the conditions for the laser-induced synthesis of nickel microstructures (Ni electrode). Then, we deposited gold on the surface of a nickel microline from a DMF solution containing 1 mM chloro(triphenylphosphine)-gold(I) upon the focused 532 nm laser light. Similarly, we modified the surface of the Ni electrode with platinum structures synthesized from a DMF solution with 1 mM dichloro(dicyclopentadienyl)platinum(II). The compositions of the solutions used for these experiments are presented in Table 1. Other experimental conditions can be found in the previous section.

Figure 4 illustrates SEM images of Ni, Ni-Au, and Ni-Pt. As one can see, these electrode materials have a well-developed

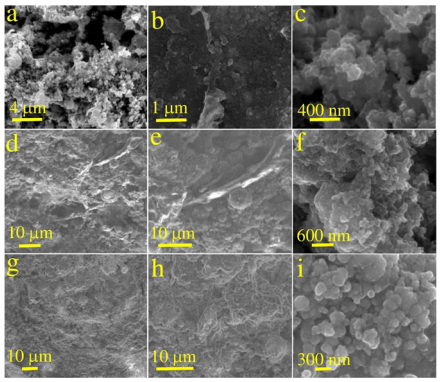

Figure 4. SEM images of Ni (a−c), Ni-Au (d−f), and Ni-Pt (g−i). All materials exhibit a developed morphology. The surface of the Ni electrode has a hierarchical structure with large-scale 10 μm pores and small-scale 10 nm irregularities. In turn, the Ni-Pt surface has large-scale cavities (g), small-scale pores (h), and a few tens of nanometer particles (i) in contrast to the Ni-Au electrode that reveals no obvious hierarchical structure.

porous morphology. Figure 4a demonstrates the size distribution of the submicrometer pores for the Ni electrode. As is shown, this electrode surface mainly has 750 nm pores. In turn, the surfaces of Ni and Ni-Pt have hierarchical structures consisting of large-scale cavities and small-scale pores, while the surface of the Ni-Au electrode has no obvious separation between pore sizes (Figure 4d). The data presented in Figure 4e,h indicate that, in the range of up to 10 μm, the average pore size for Ni-Pt is smaller than that for the Ni-Au electrode. In addition, according to Figure 5a, the average pore size for

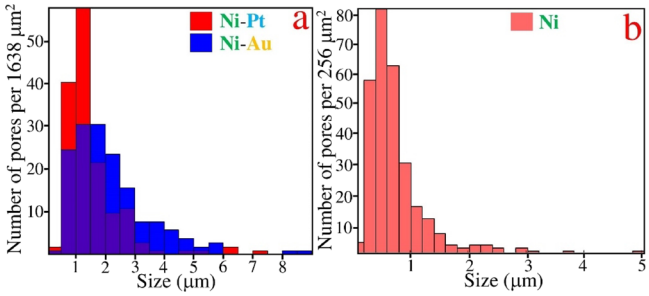

Figure 5. Size distribution (a, b) of the sub-10 μm pores calculated from Figure 4e,h and Figure 4a, respectively. The obtained data indicate that the average size of the pores of the Ni-Pt electrode material is smaller than that observed for Ni-Au. However, the number of the small-size pores (1−1.5 μm) in the Ni-Pt electrode is significantly higher than that estimated for Ni-Au. The pure Ni electrode has a mean irregularity size of 750 nm.

the Ni-Pt electrode (1.5 μm) is lower than that observed for Ni-Au (2.3 μm), whereas the number of the small-size pores for Ni-Pt is significantly higher than that of the pores with same size for the Ni-Au electrode material. Thus, the surface of Ni-Pt is more complex and developed than the surface of the Ni-Au electrode, and we assume that impedance measurements for Ni-Pt should demonstrate lower values of non-ideality parameters α in comparison with the Ni-Au electrode material.

https://doi.org/10.1021/acsomega.1c01880
ACS Omega 2021, 6, 18099−18109

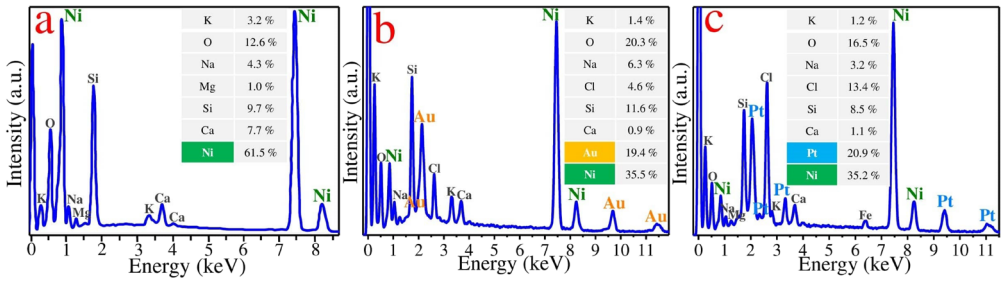

Figure 6. Results of EMP analysis of Ni (a), Ni-Au (b), and Ni-Pt (c). The mean weight (%) distributions of the elements observed in these electrode materials are shown in the legends.

The results of EMP analysis of Ni, Ni-Au, and Ni-Pt electrodes are shown in Figure 6. These data justify the element composition of these electrodes. The presence of K, Ca, O, Na, Si, and Cl in the spectra can be associated with the substrate material (glass).

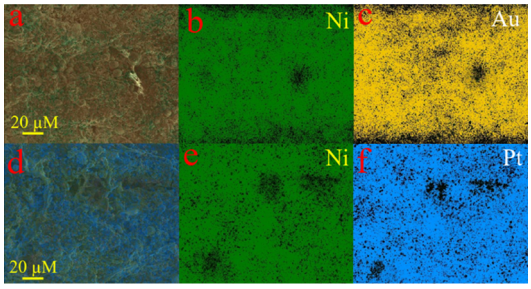

Figure 7. EDX mapping of the Ni-Au electrode: (a) superposition of the EDX maps from panels (b, c); (b) Ni map (green) and (c) Au map (yellow). EDX mapping of the Ni-Pt electrode: (d) superposition of the EDX maps from panels (e, f); (e) Ni map (green) and (f) Pt map (light blue).

The results of the elemental studies were confirmed by X-ray diffraction analysis. The XRD patterns of the synthesized electrode materials demonstrated in Figure 8 mostly reveal the presence of the metallic phases. Indeed, Ni microstructures modified with Au and Pt (Figure 8b,c) have only an insignificant amount of nickel dioxide (NiO), whereas pure Ni has no oxide impurities (Figure 8a). This observation is consistent with the low electrical resistance of all the discussed materials (~10, ~17, and ~19 Ω for Ni, Ni-Au, and Ni-Pt, respectively). It should also be noted that we were able to fabricate Ni-based microstructures with better morphology in comparison with Ni-Au structures previously deposited on glass-ceramics[50] using a higher scanning speed, lower laser power, and lower concentration of the components.

We also performed EDX mapping of the modified Ni electrodes synthesized in the current work (Figure 7). Figure 7 demonstrates the distribution of Ni, Au, and Pt along the bimetallic electrode surface.

Further morphology analysis of the produced electrode materials was performed using impedance spectroscopy. Figure 8 and Table 2 illustrate the admittance spectra of these materials and the results of their approximation. One can see that the spectra of all three electrodes could be perfectly fitted by a two-branch scheme, as shown in Figure 2. The data presented in Table 2 indicate that the electrode spectra could be described by means of the capacitance dispersion effect[46−48] because all non-ideality parameters α are significantly different from the unity (we fixed α_1 as equal to 0.5 for Ni-Pt during approximation because its value was stable for all experiments). As it was assumed by SEM analysis, the Ni-Pt electrode has lower α values than Ni-Au because it has a smaller pore size and the average number of the small-size pores for Ni-Pt is significantly higher than that calculated for the Ni-Au electrode. Moreover, the perfect fit of Ni-Pt spectra with fixed α_1 = 0.5 also indicated that this electrode type has an ideal porous structure.[46] The existence of two *R*-CPE branches with different α-values in the admittance spectra of the Ni-Pt electrode can be explained by the presence of the large-scale cavities and small-size pores on the electrode surface (Figure 4e,h). Contrary to Ni and Ni-Pt electrodes, Ni-Au exhibits similar α-values for both *R*-CPE branches. In fact, this effect could indicate that the two-branch model (Figure 2) overestimates the spectrum. Indeed, if $\alpha_1 = \alpha_2$, then it is possible to have the situation at which $R_1/R_2 = W_2/W_1$ holds. Under such conditions, the scheme shown in Figure 2 is degenerate into a one-branch *R*-CPE circuit; as a result, the elements of the two-branched scheme separately lose their physical meaning. However, the conditions at which $R_1/R_2 = W_2/W_1$ do not hold, as clearly seen from Table 2 (Ni-Au). Thus, the existence of two *R*-CPE branches in Ni-Au can be associated not only with a complex morphology of the

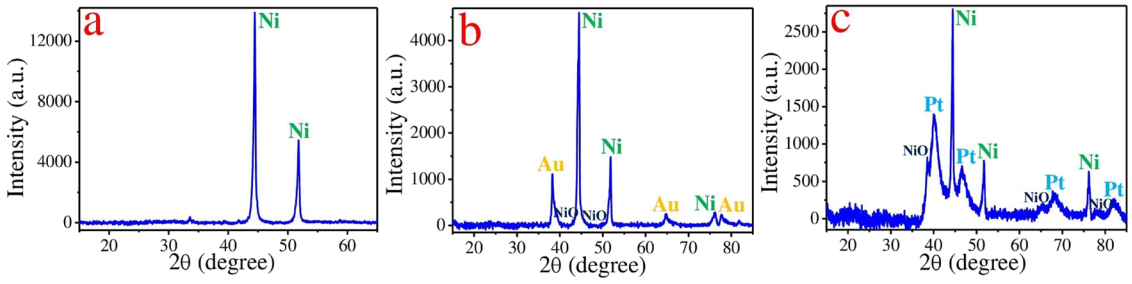

Figure 8. XRD patterns of (a) Ni, (b) Ni-Au, and (c) Ni-Pt electrodes deposited on glass.

https://doi.org/10.1021/acsomega.1c01880
ACS Omega 2021, 6, 18099−18109

Table 2. Results of Approximation for Ni, Ni-Au, and Ni-Pt Electrodes[a]

		R_1 (Ω)	R_2 (Ω)	W_1 (S $s^{\alpha 1}$)	W_2 (S $s^{\alpha 2}$)	α_1	α_2
Ni	value	2370	1840	1.31×10^{-6}	6.1×10^{-7}	0.652	0.556
	CI	60	30	5.0×10^{-8}	4.0×10^{-8}	0.005	0.08
Ni-Au	value	1600	9000	6.3×10^{-6}	1.0×10^{-7}	0.685	0.68
	CI	30	1000	2.0×10^{-7}	4.0×10^{-8}	0.005	0.04
Ni-Pt	value	3760	6800	9.3×10^{-7}	1.7×10^{-6}	0.5	0.588
	CI	60	300	4.0×10^{-8}	1.0×10^{-7}	exact	0.009

[a]Here, CI is 99.9% confidence intervals.

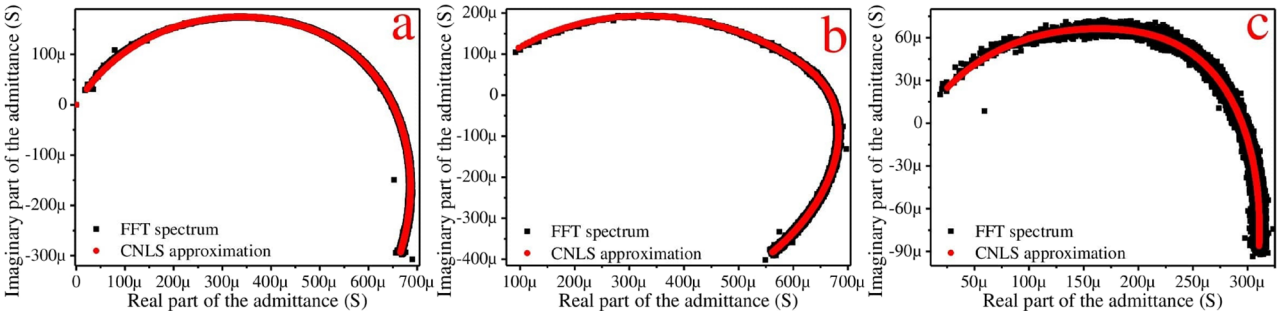

Figure 9. Admittance spectra of (a) Ni, (b) Ni-Au, and (c) Ni-Pt microstructures deposited on glass. The equivalent scheme presented in Figure 2 completely describes small signal electrical properties of these electrodes.

electrode surface but also with different resistive and capacitive properties of different electrode structures and sections, for example, due to their different elemental compositions. On the other hand, similar α-values for the Ni-Au electrode can testify the absence of the hierarchical structure of the electrode surface opposite to Ni and Ni-Pt, non-ideality parameters of which have different values due to the hierarchical nature of their electrode surfaces (Figure 4).

It is known that, in the bimetallic sensor systems, the presence of a precious metal such as gold or platinum as one of the components significantly increases the biocompatibility of such systems in comparison with monometallic systems consisting of non-precious metals.[10] In this work, we decided to investigate the influence of morphology on the toxicity of Ni structures modified with Au and Pt. Figure 10 shows the biocompatibility of Ni-Au and Ni-Pt electrodes with the HeLa cells. As one can see, these electrodes are non-toxic because both of them have living cells on their surfaces. Indeed, dead cells exhibit a yellow color as a mix of the green DiBAC channel and red propidium iodide channel, whereas living cells reveal only a green color. At the same time, the Ni-Au electrode has a much better cell adhesion than Ni-Pt. Perhaps, this difference is due to the more complex morphology of the Ni-Pt surface in comparison with Ni-Au, which was confirmed by SEM analysis and impedance spectroscopy. A similar behavior was shown by different cytotoxicities of AuNPs and PtNPs that were interpreted by the difference in the diameter of nanoparticles, where smaller PtNPs reveal greater cytotoxicity.[51] Additionally, the obtained images demonstrate that the cell adhesion on the electrode surface is different from that observed on the flat surface of a substrate (glass). Indeed, the cells on the electrodes have a spherical-like shape in contrast to the fusiform shape of the HeLa cells on the flat surface. This effect could be caused by a non-regular electrode surface, which makes it difficult for a cell to take a fusiform shape.

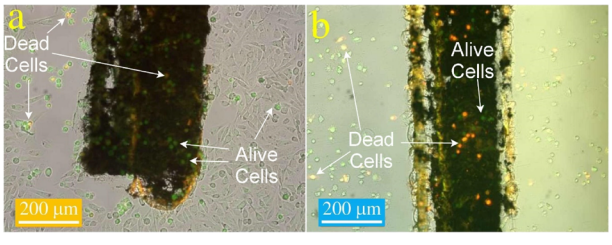

Figure 10. Biocompatibility of the Ni-Au (a) and Ni-Pt (b) electrode materials. The pseudocolor images were obtained as superposition of three photographs: (i) taken in visible light of the transmitted light mode (grayscale); (ii) the DiBAC fluorescence (green channel, membrane visualization); (iii) the propidium iodide fluorescence (red channel, dead cell nuclei visualization). One can see that both electrodes contain living cells; however, Ni-Au microstructures demonstrate better cell adhesion properties than Ni-Pt.

As is known, the development of the electrode surface determines its electrocatalytic activity. Therefore, we conducted a comparative study of the influence of morphology on the enzyme-free glucose sensing of the fabricated Ni-based electrodes. Figure 11a illustrates typical cyclic voltammograms (CVs) of these electrode materials recorded in a solution of 0.1 M NaOH. The recorded CV area can be directly related to the degree of development of the electrode surface and its sensitivity. According to Figure 11a, it is clear that the modification of the Ni electrode with Pt leads to the most prominent increase in the area of the cyclic voltammogram curve. Indeed, the Ni-Pt electrode exhibits the strongest current response for oxidation of glucose, assuming that this material may display better electrocatalytic performance. Figure 11b shows the CVs of Ni-Pt recorded in the background solution (0.1 M NaOH) containing 100 and 1000 μM D-glucose, which demonstrate the gradual increase in the oxidation current with the increase in the glucose concentration.

Typical amperometric responses of the Ni-based electrodes are shown in Figure 11c. As one can see, Ni-Pt reveals the highest current response upon successive additions of D-

https://doi.org/10.1021/acsomega.1c01880
ACS Omega 2021, 6, 18099−18109

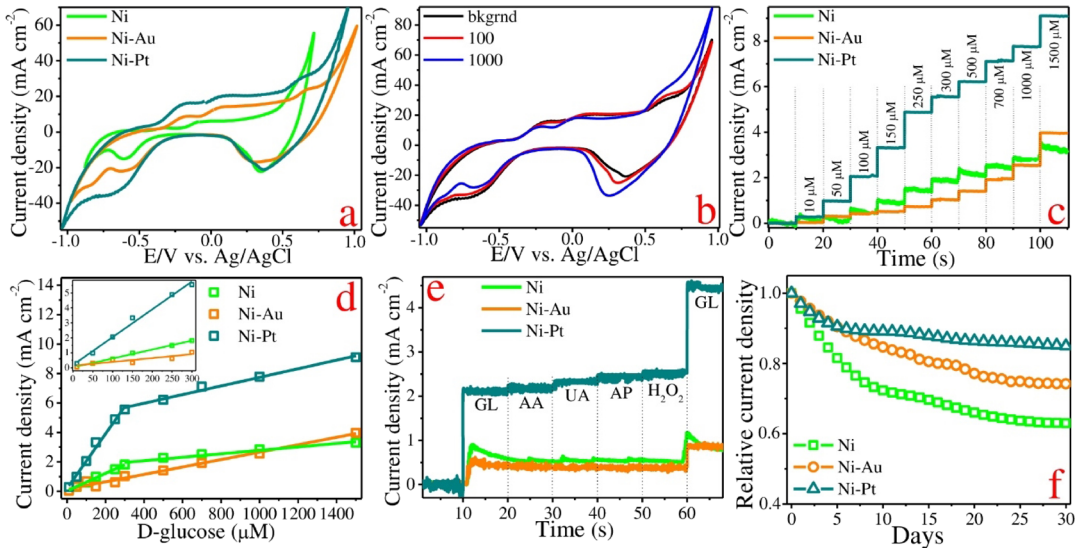

Figure 11. (a) Cyclic voltammograms (CVs) of the fabricated electrode materials recorded in 0.1 M NaOH. (b) CVs of the Ni-Pt electrode obtained in a background solution with two concentrations of D-glucose (shown in μM, top left corner); (c) amperometric current of the fabricated electrodes recorded in the presence of different concentrations of D-glucose at potentials of 0.60 V (for Ni), 0.64 V (for Ni-Au), and 0.62 V (for Ni-Pt); (d) linear ranges of enzymeless D-glucose detections of Ni, Ni-Au, and Ni-Pt electrodes; (e) selectivity of the fabricated materials observed upon the consecutive addition of 100 μM D-glucose (GL), 30 μM ascorbic acid (AA), 30 μM uric acid (UA), 30 μM 4-acetamidophenol (AP), and 30 μM hydrogen peroxide (H_2O_2) to a background solution of 0.1 M NaOH; (f) long-run stability of the Ni-based electrodes toward non-enzymatic D-glucose sensing tested for 1 month.

glucose of different concentrations to a background solution at an applied potential of 0.62 V. Figure 9d presents the calibration curves and their linear fits. It was demonstrated here that Ni and Ni-Pt electrodes have two linear regions of glucose concentration opposite to Ni-Au, which has only one linear range. In the first linear region, the amperometric current increases rapidly with the increase in the glucose concentration, whereas within the second linear region, the growth of the analytical response is noticeably slowing down. Such a behavior can be attributed to the presence of two types of pores on the hierarchical surface of Ni and Ni-Pt electrodes, the smallest of which exhibits high sensitivity at low glucose concentrations up to 300 μM. On the other hand, at higher concentrations of glucose, the sensitivity drastically drops, probably due to the stronger adsorption of the intermediates forming during the reaction of the electrocatalytic glucose oxidation.[52] It should be noted that Ni-Pt with the mostly developed surface area demonstrates the steepest slope on the calibration curves, as shown in Figure 11d, i.e., it exhibits the highest sensitivity among all fabricated materials within the glucose concentrations up to 300 μM. The calculated sensitivities of Ni-Pt are 18,570 and 2929 μA mM^{-1} cm^{-2}; the intervals of linear regions are 10−300 and 300−1500 μM. The detection limits are 0.14 and 0.19 μM, which were calculated as LOD = $3S/b$. Here, S is the standard deviation from linearity and b is the slope of the calibration curve (shown in Figure 11d). The analytical performance of the Ni-based electrodes fabricated in this work and other non-enzymatic glucose sensors is compared in Table 3. It is clear that Ni-Pt exhibits a number of advantages over the compared counterparts mostly related to its high sensitivity and low detection limit. This excellent sensing performance of Ni-Pt electrode can be associated with the well-developed morphology of this material and catalytic synergy between Ni and Pt. Indeed, it was found that bimetallic catalytic micro- or nanostructures based on Pt are favorable due to the presence of a second metal atom that can synergistically facilitate catalytic activity and stability via electronic, alloying, or strain effects and availability of a greater number of catalytically active sites.[27,32]

Table 3. Electrochemical Properties of the Fabricated Microstructures and Similar Electrode Materials Used for Non-Enzymatic Glucose Sensing

Electrode material	Linear range (μM)	LOD (μM)	Sensitivity (μA mM^{-1} cm^{-2})	Refs
Ni	10−300 and 300−1500	0.09 and 0.32	5953 and 1180	this work
Ni-Au	10−1500	0.12	2542	this work
Ni-Pt	10−300 and 300−1500	0.14 and 0.19	18,570 and 2929	this work
Ni nanowire arrays	0.5−7000	0.1	1043	55
Ni nanoparticles on straight multiwalled carbon nanotubes	1−1000	0.5	1438	56
Ni nanoparticles/porous carbon	15−6450	4.8	207.3	57
Au/Ni multilayer nanowire array	0.25−2000 2000−5500	0.1	3372 1906	41
NiAu alloy dendrites on carbon papers	1−3000	0.2	4035.4	42
AuNi nanodendrite arrays	5−15,000	3	3727.7	58
PtNi alloy nanocatalysts on carbon	2−420	1	1795.1	59
Pt-Ni nanoclusters	0−15,000	0.3	940	60
PtNi nanoparticle-graphene nanocomposites	0−35,000	10	20.42	38

Possible reactions involved in the process of the electro-oxidation of glucose under alkaline conditions on the surfaces of Ni electrodes modified with Au and Pt can be shown as follows:[9,10,42]

https://doi.org/10.1021/acsomega.1c01880
ACS Omega 2021, 6, 18099−18109

$$Ni + 2OH^- \leftrightarrow Ni(OH)_2 + 2e^- \quad (1)$$

$$Ni(OH)_2 + OH^- \leftrightarrow NiOOH + H_2O + e^- \quad (2)$$

$$NiOOH + glucose \leftrightarrow Ni(OH)_2 + glucolactone \quad (3)$$

$$Au + OH^- \leftrightarrow AuOH + e^- \quad (4)$$

$$AuOH + glucose \leftrightarrow Au + glucolactone \quad (5)$$

$$Pt + 2OH^- \leftrightarrow Pt(OH)_2 + 2e^- \quad (6)$$

$$Pt(OH)_2 + glucose \leftrightarrow Pt + glucolactone \quad (7)$$

$$2Pt + O_2 \leftrightarrow 2PtO \quad (8)$$

$$PtO + glucose \leftrightarrow Pt + glucolactone \quad (9)$$

As it was mentioned above, pure Ni electrodes have a number of drawbacks, including their inability to operate in the physiological environment (pH = 7.4). According to the literature, oxidation of glucose on the surface of Ni involves NiOOH catalysis, which is highly dependent on the concentration of OH^- anions.[9,53] On the other hand, the bimetallic systems can drastically facilitate the electrooxidation of glucose via the synergetic effect.[9,10] For example, Pt- and Au-based materials can be used as platforms for glucose sensing, providing better sensitivity, selectivity, and stability. Moreover, the most significant advantage of the Pt-based electrodes in contrast to other bimetallic sensing materials, including many the Au-based ones, is their great catalytic performance under neutral and alkaline pH conditions. In this work, we tested Ni-Pt and Ni-Au electrodes toward non-enzymatic glucose sensing in alkaline solution (0.1 M NaOH). Indeed, in many studies, glucose sensors are examined in alkaline solutions because of the natural enhancement of their catalytic properties. The reasons of such behavior are the following: low pH leads to corrosion, whereas the amount of reactive OH^- is higher at higher pH values. In addition, high pH conditions improve the selectivity of metal-based electrodes due to their negatively charged surfaces that repel many interfering species such as chloride, sulfate, phosphate, ascorbic acid, and others. Our observations on Pt- and Au-containing Ni electrodes are consistent with those observed by many authors for similar materials.[9,10] Such consistency was also demonstrated by the electrochemical experiments performed at neutral pH (0.1 M PBS (phosphate buffer); Figure 12).

In general, the better catalytic performance of Ni-Pt in both NaOH and PBS with respect to Ni-Au can be explained by its less dependence on OH^- ion concentration and a more negatively charged surface. The higher catalytic activity of the Ni-Pt electrode may also be associated with a more developed morphology (i.e., greater porosity) of this material. Moreover, to some extent, weak chemisorption of gold due to filled d-orbitals as one of the stages of glucose electrooxidation can also reduce the catalytic performance of the Ni-Au electrode in comparison with Ni-Pt.[9]

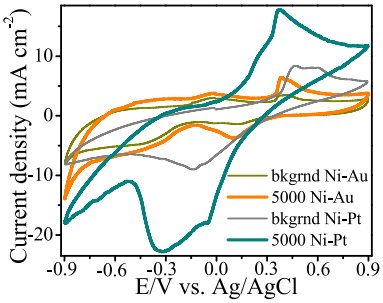

Figure 12. Cyclic voltammograms (CVs) of Ni-Pt and Ni-Au electrodes obtained in the background solution (0.1 M PBS (phosphate buffer)) with the addition of 5000 μM D-glucose.

According to the results of the electrochemical studies of the synthesized nickel-containing materials in neutral and basic media, it is possible to propose a mechanism for the oxidation of glucose on their surface. Figure 13 represents a possible mechanism of glucose electrooxidation on the surface of Ni-Pt as the most promising material obtained in this work. According to the CVs obtained under neutral and alkaline conditions for this electrode material (Figures 11a and 13), and taking into account the models known from the literature[9,10,26,54] and mentioned above (reactions 1−9), we can distinguish the several potential regions of Ni electrodes modified with Au and Pt.

The first potential region ("hydrogen region") is located below −0.10 V with the anodic peaks centered at −0.21 and −0.19 V observed for Ni-Pt and Ni-Au electrodes, respectively. In this region, the dehydrogenation of the glucose molecule at the hemiacetalic carbon atom (C_1) with its further chemisorption onto the platinum or gold surfaces can be observed. As for the pure Ni electrode, in the alkaline medium, nickel exists in hydroxide form according to eq 1 that then undergoes the redox reaction with formation of the catalytically active Ni(III) oxyhydroxide species (see eq 2). The second potential region is located between −0.10 and 0.48 V (for Ni-Pt and Ni-Au) and between −0.20 and 0.43 V (for Ni). This region can be attributed to the "double-layer region", in which the anodic peaks centered at 0.09, 0.08, and −0.06 V exhibited by Ni-Pt, Ni-Au, and Ni, respectively, correspond to the electrooxidation of the chemisorbed species. Here, the dissociation of water is followed by the release of the hydroxide anions that were absorbed by the surface of an electrode forming the catalytic hydroxide premonolayer (eqs 4 and 6). The latter accelerates the electrooxidation of the chemisorbed glucose molecule via the reactions shown in eqs 3, 5, and 7. In the third potential region, the anodic peaks centered at 0.62 V (for Ni-Pt), 0.64 V (for Ni-Au), and 0.60 V (for Ni) are referred to further oxidation of the bulk glucose solution with formation of gluconolactone and subsequently gluconic acid. In addition, in the case of Ni-Pt, this range of potentials can be associated with the "oxygen region", in which the Pt surface is covered by a monolayer of the adsorbed oxygen forming PtO films that reveal electrocatalytic activity toward glucose oxidation (eqs 8 and 9). Finally, the peaks centered at −0.65 and 0.36 V can be attributed to the cathodic oxidation processes.

The selectivity of the fabricated electrode materials toward enzymeless glucose sensing was estimated in the presence of several interferents, including ascorbic acid (AA), urea (UA), 4-acetamidophenol (AP), and hydrogen peroxide (H_2O_2) (Figure 11e). According to the obtained results, all three electrodes demonstrated much stronger amperometric responses with respect to glucose in contrast to those observed for additives of the interfering substances. This suggests that Ni-based electrodes generally have a fairly decent selectivity for the specific glucose detection, showing the best result in the case of Ni-Pt.

https://doi.org/10.1021/acsomega.1c01880
ACS Omega 2021, 6, 18099−18109

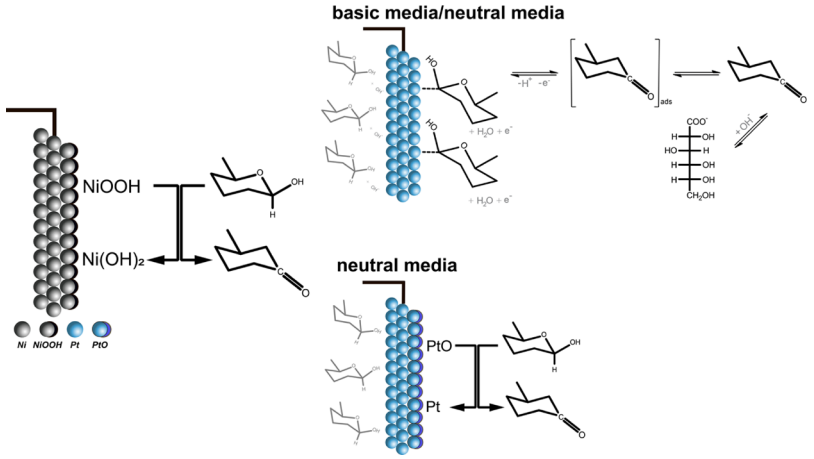

Figure 13. Schematic illustration of a possible mechanism for oxidation of glucose on the surface of the Ni-Pt electrode.

The long-run stability of the nickel-based non-enzymatic glucose sensors stored at the room temperature was tested for 1 month (Figure 11f). For that reason, we evaluated the change of the relative current density (I_x/I_0) over the mentioned time period. Here, I_x and I_0 are the current densities exhibited by the fabricated electrode materials upon the addition of 100 μM D-glucose and recorded on days x and zero, respectively. It was found that the modification of the surface of the Ni electrode with precious metals significantly improves its stability. In turn, the relative current density of the Ni-Pt electrode remained not less than 85% of its initial value for 1 month, demonstrating the highest level of stability among the studied electrode materials.

CONCLUSIONS

In this work, we synthesized Ni microstructures and conducted their modification with Au and Pt using the method of laser-induced metal deposition from a solution (LCLD). The morphological studies, the elemental and phase analysis of the fabricated metallic, and bimetallic microstructures were performed using SEM, EMP, and XRD, respectively. SEM showed that the surfaces of Ni and Ni-Pt have a hierarchical structure consisting of large-scale cavities and small-scale pores, while the surface of the Ni-Au electrode has no obvious separation between pore sizes. Thus, the surface of Ni modified with Pt is more complex and developed than that of Ni structures modified with Au. This was confirmed by impedance measurements demonstrating lower values of non-ideality parameters α for Ni-Pt. According to EMP and XRD analysis, Ni microstructures modified with Au and Pt reveal the presence of mostly the metallic phases and have only insignificant amounts of nickel dioxide (NiO), whereas pure Ni has no oxide impurities. The biocompatibility studies demonstrated that the Ni-Au electrode has a much better cell adhesion than Ni-Pt. We associate this to the higher irregularity of the surface of the Ni-Pt electrode in comparison with Ni modified with Au. In turn, an opposite trend was observed for the electrochemical properties of the fabricated electrode materials. Indeed, the Ni-based microstructures with a more developed surface area revealed better catalytic performance toward non-enzymatic glucose detection. In this regard, the modification of the Ni surface with Pt results in the most significant enhancement of the glucose sensing characteristics, probably due to the greater synergetic catalytic effect and the presence of a greater number of active sites. Moreover, the electrode materials with a hierarchical structure such as Ni and Ni-Pt exhibited two linear regions of glucose concentration, and, as a result, two detection limits and two sensitivity levels. For Ni-Pt that outperformed others, these parameters are 10–300 and 300–1500 μM, 0.14 and 0.19 μM, and 18,570 and 2929 μA mM^{-1} cm^{-2}. This can be explained by the presence of two types of pores on the surface of these electrodes, the smallest of which exhibits high sensitivity within the range of low concentrations of glucose. However, at higher glucose concentrations, the sensitivity significantly decreases, probably due to the stronger adsorption of the intermediates forming during the electrocatalytic glucose oxidation. In conclusion, it should be noted that the results obtained in the current study could be quite useful for the design of materials with low cell toxicity and high catalytic performance.

AUTHOR INFORMATION

Corresponding Author

Ilya I. Tumkin − *Saint Petersburg State University, St. Petersburg 199034, Russia;* orcid.org/0000-0003-4841-7529; Email: i.i.tumkin@spbu.ru

Authors

Evgeniia M. Khairullina − *Saint Petersburg State University, St. Petersburg 199034, Russia*

Daniil D. Stupin − *Nanotechnology Research and Education Centre RAS, Saint Petersburg Academic University, St. Petersburg 194021, Russia*

Alexandra V. Smikhovskaia − *Saint Petersburg State University, St. Petersburg 199034, Russia*

Andrey S. Mereshchenko − *Saint Petersburg State University, St. Petersburg 199034, Russia;* orcid.org/0000-0001-9390-1446

Alexey I. Lihachev − *Ioffe Institute, St. Petersburg 194021, Russian Federation*

Andrey V. Vasin − *Peter the Great St. Petersburg Polytechnic University, 195251 St. Petersburg, Russia*

Mikhail N. Ryazantsev − *Saint Petersburg State University, St. Petersburg 199034, Russia; Nanotechnology Research and Education Centre RAS, Saint Petersburg Academic University, St. Petersburg 194021, Russia;* orcid.org/0000-0003-3413-1706

Maxim S. Panov − *Saint Petersburg State University, St. Petersburg 199034, Russia*

Complete contact information is available at:

https://doi.org/10.1021/acsomega.1c01880
ACS Omega 2021, 6, 18099−18109

https://pubs.acs.org/10.1021/acsomega.1c01880

Notes

The authors declare no competing financial interest.

E.M.K. provided the synthesis and investigation. I.I.T. provided the funding acquisition and project administration. A.V.S. provided the validation and investigation. D.D.S. provided the methodology and investigation. A.S.M. and A.I.L. provided the investigation and formal analysis. A.V.V. provided the validation and supervision. M.N.R. provided the writing by reviewing and editing the manuscript and supervision. M.S.P. provided the conceptualization and writing of the original draft.

■ ACKNOWLEDGMENTS

I.I.T., A.V.S., E.M.K., and M.S.P. acknowledge the Russian Science Foundation (grant 20-79-10075). The authors would like to thank the SPbSU Nanotechnology Interdisciplinary Centre, Centre for Optical and Laser Materials Research, and Centre for X-ray Diffraction Studies. SEM characterization was performed using equipment owned by the Federal Joint Research Center "Material science and characterization in advanced technology".

■ REFERENCES

(1) Wei, F.; Patel, P.; Liao, W.; Chaudhry, K.; Zhang, L.; Arellano-Garcia, M.; Hu, S.; Elashoff, D.; Zhou, H.; Shukla, S.; Shah, F.; Ho, C.-M.; Wong, D. T. Electrochemical Sensor for Multiplex Biomarkers Detection. *Clin. Cancer Res.* **2009**, *15*, 4446−4452.

(2) Heikenfeld, J.; Jajack, A.; Rogers, J.; Gutruf, P.; Tian, L.; Pan, T.; Li, R.; Khine, M.; Kim, J.; Wang, J.; Kim, J. Wearable Sensors: Modalities, Challenges, and Prospects. *Lab Chip* **2018**, *18*, 217−248.

(3) Trial, C. Effect of Intensive Therapy on the Development and Progression of Diabetic Nephropathy in the Diabetes Control and Complications Trial. *Kidney Int.* **1995**, *47*, 1703−1720.

(4) Sehit, E.; Altintas, Z. Significance of Nanomaterials in Electrochemical Glucose Sensors: An Updated Review (2016-2020). *Biosens. Bioelectron.* **2020**, *159*, 112165.

(5) Bakker, E. Electrochemical Sensors. *Anal. Chem.* **2004**, *76*, 3285−3298.

(6) Si, Y.; Lao, J.; Zhang, X.; Liu, Y.; Cai, S.; Gonzalez-Vila, A.; Li, K.; Huang, Y.; Yuan, Y.; Caucheteur, C.; Guo, T. Electrochemical Plasmonic Fiber-Optic Sensors for Ultra-Sensitive Heavy Metal Detection. *J. Lightwave Technol.* **2019**, *37*, 3495−3502.

(7) Revathi, C.; Rajendra Kumar, R. T. *Enzymatic and Nonenzymatic Electrochemical Biosensors*; Elsevier Ltd: 2019. DOI: 10.1016/B978-0-08-102577-2.00007-5.

(8) Ferri, S.; Kojima, K.; Sode, K. Review of Glucose Oxidases and Glucose Dehydrogenases: A Bird's Eye View of Glucose Sensing Enzymes. *J. Diabetes Sci. Technol.* **2011**, *5*, 1068−1076.

(9) Toghill, K. E.; Compton, R. G. Electrochemical Non-Enzymatic Glucose Sensors: A Perspective and an Evaluation. *Int. J. Electrochem. Sci.* **2010**, *5*, 1246−1301.

(10) Hwang, D. W.; Lee, S.; Seo, M.; Chung, T. D. Recent Advances in Electrochemical Non-Enzymatic Glucose Sensors − A Review. *Anal. Chim. Acta* **2018**, *1033*, 1−34.

(11) Li, G. Direct Laser Writing of Graphene Electrodes. *J. Appl. Phys.* **2020**, *127*, No. 010901.

(12) Mizoshiri, M.; Arakane, S.; Sakurai, J.; Hata, S. Direct Writing of Cu-Based Micro-Temperature Detectors Using Femtosecond Laser Reduction of CuO Nanoparticles. *Appl. Phys. Express* **2016**, *9*, No. 036701.

(13) Gao, J.; Shao, C.; Shao, S.; Bai, C.; Khalil, U. R.; Zhao, Y.; Jiang, L.; Qu, L. Laser-Assisted Multiscale Fabrication of Configuration-Editable Supercapacitors with High Energy Density. *ACS Nano* **2019**, *13*, 7463−7470.

(14) Mizoshiri, M.; Nishitani, K.; Hata, S. Effect of Heat Accumulation on Femtosecond Laser Reductive Sintering of Mixed CuO/NiO Nanoparticles. *Micromachines* **2018**, *9*, 264.

(15) Yang, Y. L.; Hsu, C. C.; Chang, T. L.; Kuo, L. S.; Chen, P. H. Study on Wetting Properties of Periodical Nanopatterns by a Combinative Technique of Photolithography and Laser Interference Lithography. *Appl. Surf. Sci.* **2010**, *256*, 3683−3687.

(16) Hong, M. H.; Huang, S. M.; Luk'yanchuk, B. S.; Chong, T. C. Laser Assisted Surface Nanopatterning. *Sensors Actuators, A Phys.* **2003**, *108*, 69−74.

(17) Zhang, J.; Chaker, M.; Ma, D. Pulsed Laser Ablation Based Synthesis of Colloidal Metal Nanoparticles for Catalytic Applications. *J. Colloid Interface Sci.* **2017**, *489*, 138−149.

(18) Kochemirovsky, V. A.; Skripkin, M. Y.; Tveryanovich, Y. S.; Mereshchenko, A. S.; Gorbunov, A. O.; Panov, M. S.; Tumkin, I. I.; Safonov, S. V. Laser-Induced Copper Deposition from Aqueous and Aqueous−Organic Solutions: State of the Art and Prospects of Research. *Russ. Chem. Rev.* **2015**, *84*, 1059−1075.

(19) Lozhkina, O. A.; Panov, M. S.; Logunov, L. S.; Tumkin, I. I.; Gordeychuk, D. I.; Kochemirovsky, V. A. Aluminum Chloride Reveals the Catalytic Activity towards Laser-Induced Deposition of Copper from Water-Based Solutions. *Int. J. Electrochem. Sci.* **2015**, *10*, 6084−6091.

(20) Smikhovskaia, A. V.; Panov, M. S.; Tumkin, I. I.; Khairullina, E. M.; Ermakov, S. S.; Balova, I. A.; Ryazantsev, M. N.; Kochemirovsky, V. A. In Situ Laser-Induced Codeposition of Copper and Different Metals for Fabrication of Microcomposite Sensor-Active Materials. *Anal. Chim. Acta* **2018**, *1044*, 138−146.

(21) Smikhovskaia, A. V.; Andrianov, V. S.; Khairullina, E. M.; Lebedev, D. V.; Ryazantsev, M. N.; Panov, M. S.; Tumkin, I. I. In Situ Laser-Induced Synthesis of Copper-silver Microcomposite for Enzyme-Free D-Glucose and L-Alanine Sensing. *Appl. Surf. Sci.* **2019**, *488*, 531−536.

(22) Panov, M. S.; Vereshchagina, O. A.; Ermakov, S. S.; Tumkin, I. I.; Khairullina, E. M.; Skripkin, M. Y.; Mereshchenko, A. S.; Ryazantsev, M. N.; Kochemirovsky, V. A. Non-Enzymatic Sensors Based on in Situ Laser-Induced Synthesis of Copper-Gold and Gold Nano-Sized Microstructures. *Talanta* **2017**, *167*, 201−207.

(23) Baranauskaite, V. E.; Novomlinskii, M. O.; Tumkin, I. I.; Khairullina, E. M.; Mereshchenko, A. S.; Balova, I. A.; Panov, M. S.; Kochemirovsky, V. A. In Situ Laser-Induced Synthesis of Gas Sensing Microcomposites Based on Molybdenum and Its Oxides. *Compos. Part B Eng.* **2019**, *157*, 322−330.

(24) S. Panov, M.; M. Khairullina, E.; S. Vshivtcev, F.; N. Ryazantsev, M.; I. Tumkin, I. Laser-Induced Synthesis of Composite Materials Based on Iridium, Gold and Platinum for Non-Enzymatic Glucose Sensing. *Materials* **2020**, *13*, 3359.

(25) Panov, M. S.; Grishankina, A. E.; Stupin, D. D.; Lihachev, A. I.; Mironov, V. N.; Strashkov, D. M.; Khairullina, E. M.; Tumkin, I. I.; Ryazantsev, M. N. In Situ Laser-Induced Fabrication of a Ruthenium-Based Microelectrode for Non-Enzymatic Dopamine Sensing. *Materials* **2020**, *13*, 5385−5311.

(26) Park, S.; Boo, H.; Chung, T. D. Electrochemical Non-Enzymatic Glucose Sensors. *Anal. Chim. Acta* **2006**, *556*, 46−57.

(27) Dolinska, J.; Kannan, P.; Sobczak, J. W.; Opallo, M. Glucose Electrooxidation in Bimetallic Suspensions of Nanoparticles in Alkaline Media. *ChemElectroChem* **2015**, *2*, 1199−1205.

(28) Mereshchenko, A. S.; Olshin, P. K.; Karabaeva, K. E.; Panov, M. S.; Wilson, R. M.; Kochemirovsky, V. A.; Skripkin, M. Y.; Tveryanovich, Y. S.; Tarnovsky, A. N. Mechanism of Formation of Copper(II) Chloro Complexes Revealed by Transient Absorption Spectroscopy and DFT/TDDFT Calculations. *J. Phys. Chem. B* **2015**, *119*, 8754−8763.

(29) Saei, A. A.; Dolatabadi, J. E. N.; Najafi-Marandi, P.; Abhari, A.; de la Guardia, M. Electrochemical Biosensors for Glucose Based on Metal Nanoparticles. *TrAC - Trends Anal. Chem.* **2013**, *42*, 216−227.

(30) Qiu, H.; Huang, X. Effects of Pt Decoration on the Electrocatalytic Activity of Nanoporous Gold Electrode toward

Glucose and Its Potential Application for Constructing a Non-enzymatic Glucose Sensor. *J. Electroanal. Chem.* **2010**, *643*, 39−45.
(31) Niu, X.; Li, X.; Pan, J.; He, Y.; Qiu, F.; Yan, Y. Recent Advances in Non-Enzymatic Electrochemical Glucose Sensors Based on Non-Precious Transition Metal Materials: Opportunities and Challenges. *RSC Adv.* **2016**, *6*, 84893−84905.
(32) Xu, Y.; Zhang, B. Recent Advances in Porous Pt-Based Nanostructures: Synthesis and Electrochemical Applications. *Chem. Soc. Rev.* **2014**, *43*, 2439−2450.
(33) Li, N.; Li, Q.; Yuan, M.; Guo, X.; Zheng, S.; Pang, H. Synthesis of $Co_{0.5}Mn_{0.1}Ni_{0.4}C_2O_4{\cdot}n\ H_2O$ Micropolyhedrons: Multimetal Synergy for High-Performance Glucose Oxidation Catalysis. *Chem. - Asian J.* **2019**, *14*, 2259−2265.
(34) Hong, J. W.; Kim, Y.; Kwon, Y.; Han, S. W. Noble-Metal Nanocrystals with Controlled Facets for Electrocatalysis. *Chem. - Asian J.* **2016**, *11*, 2224−2239.
(35) Arjona, N.; Trejo, G.; Ledesma-García, J.; Arriaga, L. G.; Guerra-Balcázar, M. An Electrokinetic-Combined Electrochemical Study of the Glucose Electro-Oxidation Reaction: Effect of Gold Surface Energy. *RSC Adv.* **2016**, *6*, 15630−15638.
(36) Lei, H. W.; Wu, B.; Cha, C. S.; Kita, H. Electro-Oxidation of Glucose on Platinum in Alkaline Solution and Selective Oxidation in the Presence of Additives. *J. Electroanal. Chem.* **1995**, *382*, 103−110.
(37) Nikolaev, D. M.; Shtyrov, A. A.; Mereshchenko, A. S.; Panov, M. S.; Tveryanovich, Y. S.; Ryazantsev, M. N. An Assessment of Water Placement Algorithms in Quantum Mechanics/Molecular Mechanics Modeling: The Case of Rhodopsins' First Spectral Absorption Band Maxima. *Phys. Chem. Chem. Phys.* **2020**, *22*, 18114−18123.
(38) Gao, H.; Xiao, F.; Ching, C. B.; Duan, H. One-Step Electrochemical Synthesis of PtNi Nanoparticle-Graphene Nanocomposites for Nonenzymatic Amperometric Glucose Detection. *ACS Appl. Mater. Interfaces* **2011**, *3*, 3049−3057.
(39) Lay, B.; Coyle, V. E.; Kandjani, A. E.; Amin, M. H.; Sabri, Y. M.; Bhargava, S. K. Nickel-Gold Bimetallic Monolayer Colloidal Crystals Fabricated: Via Galvanic Replacement as a Highly Sensitive Electrochemical Sensor. *J. Mater. Chem. B* **2017**, *5*, 5441−5449.
(40) Li, C.; Wang, H.; Yamauchi, Y. Electrochemical Deposition of Mesoporous Pt-Au Alloy Films in Aqueous Surfactant Solutions: Towards a Highly Sensitive Amperometric Glucose Sensor. *Chem. - Eur. J.* **2013**, *19*, 2242−2246.
(41) Qin, L.; He, L.; Zhao, J.; Zhao, B.; Yin, Y.; Yang, Y. Synthesis of Ni/Au Multilayer Nanowire Arrays for Ultrasensitive Non-Enzymatic Sensing of Glucose. *Sens. Actuators, B* **2017**, *240*, 779−784.
(42) Zhou, J.; Yin, H.; Chen, J.; Gong, J.; Wang, L.; Zheng, Y.; Nie, Q. Electrodeposition of Bimetallic NiAu Alloy Dendrites on Carbon Papers as Highly Sensitive Disposable Non-Enzymatic Glucose Sensors. *Mater. Lett.* **2020**, *273*, 127912.
(43) Stupin, D. D.; Koniakhin, S. V.; Verlov, N. A.; Dubina, M. V. Adaptive Filtering to Enhance Noise Immunity of Impedance and Admittance Spectroscopy: Comparison with Fourier Transformation. *Phys. Rev. Appl.* **2017**, *7*, No. 054024.
(44) Carolina, N.; Hill, C. SolidState Department , Physics Laboratory ,. State TUniversity Of Utrecht , 3508 TA Utrecht (The Netherlands) Department of Physics and Astronomyo Uni ∼ Ersig ,. o f North Carolina , Chapel Hill , NC 27514 (U . S . A .) the . Solarrron : L 172 . A Com.
(45) Jorcin, J. B.; Orazem, M. E.; Pébère, N.; Tribollet, B. CPE Analysis by Local Electrochemical Impedance Spectroscopy. *Electrochim. Acta* **2006**, *51*, 1473−1479.
(46) De Levie, R. The Influence of Surface Roughness of Solid Electrodes on Electrochemical Measurements. *Electrochim. Acta* **1965**, *10*, 113−130.
(47) Kerner, Z.; Pajkossy, T. On the Origin of Capacitance Dispersion of Rough Electrodes. *Electrochim. Acta* **2000**, *46*, 207−211.
(48) Pajkossy, T. Impedance of Rough Capacitive Electrodes. *J. Electroanal. Chem.* **1994**, *364*, 111−125.
(49) Tweedale, G. Asbestos and Its Lethal Legacy. *Nat. Rev. Cancer* **2002**, *2*, 311−314.
(50) Panov, M.; Aliabev, I.; Khairullina, E.; Mironov, V.; Tumkin, I. Fabrication of Nickel-Gold Microsensor Using in Situ Laser-Induced Metal Deposition Technique. *J. Laser Micro Nanoeng.* **2019**, *14*, 266−239.
(51) Hashimoto, M.; Kawai, K.; Kawakami, H.; Imazato, S. Matrix Metalloproteases Inhibition and Biocompatibility of Gold and Platinum Nanoparticles. *J. Biomed. Mater. Res. - Part A* **2016**, *104*, 209−217.
(52) El Khatib, K. M.; Abdel Hameed, R. M. Development of Cu_2O/Carbon Vulcan XC-72 as Non-Enzymatic Sensor for Glucose Determination. *Biosens. Bioelectron.* **2011**, *26*, 3542−3548.
(53) Watanabe, T.; Einaga, Y. Design and Fabrication of Nickel Microdisk-Arrayed Diamond Electrodes for a Non-Enzymatic Glucose Sensor Based on Control of Diffusion Profiles. *Biosens. Bioelectron.* **2009**, *24*, 2684−2689.
(54) Jin, C.; Chen, Z. Electrocatalytic Oxidation of Glucose on Gold-Platinum Nanocomposite Electrodes and Platinum-Modified Gold Electrodes. *Synth. Met.* **2007**, *157*, 592−596.
(55) Lu, L. M.; Zhang, L.; Qu, F. L.; Lu, H. X.; Zhang, X. B.; Wu, Z. S.; Huan, S. Y.; Wang, Q. A.; Shen, G. L.; Yu, R. Q. A Nano-Ni Based Ultrasensitive Nonenzymatic Electrochemical Sensor for Glucose: Enhancing Sensitivity through a Nanowire Array Strategy. *Biosens. Bioelectron.* **2009**, *25*, 218−223.
(56) Nie, H.; Yao, Z.; Zhou, X.; Yang, Z.; Huang, S. Nonenzymatic Electrochemical Detection of Glucose Using Well-Distributed Nickel Nanoparticles on Straight Multi-Walled Carbon Nanotubes. *Biosens. Bioelectron.* **2011**, *30*, 28−34.
(57) Wang, L.; Zhang, Y.; Yu, J.; He, J.; Yang, H.; Ye, Y.; Song, Y. A Green and Simple Strategy to Prepare Graphene Foam-like Three-Dimensional Porous Carbon/Ni Nanoparticles for Glucose Sensing. *Sens. Actuators, B* **2017**, *239*, 172−179.
(58) Wang, L.; Zhu, W.; Lu, W.; Shi, L.; Wang, R.; Pang, R.; Cao, Y. Y.; Wang, F.; Xu, X. One-Step Electrodeposition of AuNi Nanodendrite Arrays as Photoelectrochemical Biosensors for Glucose and Hydrogen Peroxide Detection. *Biosens. Bioelectron.* **2019**, *142*, 111577.
(59) Sheng, Q.; Mei, H.; Wu, H.; Zhang, X.; Wang, S. PtxNi/C Nanostructured Composites Fabricated by Chemical Reduction and Their Application in Non-Enzymatic Glucose Sensors. *Sens Actuators B Chem* **2014**, *203*, 588−595.
(60) Zhao, Y.; Fan, L.; Hong, B.; Ren, J.; Zhang, M.; Que, Q.; Ji, J. Nonenzymatic Detection of Glucose Using Three-Dimensional PtNi Nanoclusters Electrodeposited on the Multiwalled Carbon Nanotubes. *Sens. Actuators, B* **2016**, *231*, 800−810.

https://doi.org/10.1021/acsomega.1c01880
ACS Omega 2021, 6, 18099−18109